

Asymmetric tip design for far infrared metamaterial sensor

LU Xiao-Sen, WU Xu*, WEI Xiao-Ke, WANG Jun-Jie, WANG Qi-Liang, JIN Zuan-Ming, PENG Yan
(School of Optical-Electrical and Computer Engineering, University of Shanghai for Science and Technology, Shanghai 200093, China)

Abstract: This study investigates an asymmetric tip design for a far-infrared metamaterial aimed at enhancing the Q factor and detection sensitivity. Employing the conventional double-split square ring resonator as a model, we conducted theoretical simulations to investigate the impact of different tip angles on the electric field distribution, resonance spectrum, and Q factor. The results show that the asymmetric tip increases the surface electric field of the resonator, decreases the full width at half maximum (FWHM) of the resonance peak, and increases the Q factor to over three times that of the conventional split ring. Our findings offer valuable insights for the development of highly sensitive far-infrared metamaterial sensors. Furthermore, we propose a straightforward and practical optimization approach to enhance the Q factor of conventional split ring metamaterials.

Key words: terahertz sensor, metamaterial, far infrared, Q factor

非对称针尖结构对远红外超材料谐振性能的影响研究

陆小森, 吴旭*, 魏小柯, 王俊杰, 王奇亮, 金钻明, 彭滢
(上海理工大学 光电信息与计算机工程学院, 上海 200093)

摘要: 为提高远红外超材料的品质因子 Q 和检测灵敏度, 本文研究了一种用于金属远红外超材料的非对称针尖设计。以传统双开口方形谐振环为模型, 通过理论模拟, 研究了开口狭缝针尖角度变化对其电场分布、谐振频谱以及品质因子 Q 的影响。结果表明, 非对称针尖增强了谐振环的表面电场局域性, 减小了谐振峰的半峰全宽, 并使品质因子 Q 提高到传统谐振环(非针尖设计)的三倍以上。该研究结果为开发高灵敏远红外超材料传感器提供了新的思路, 并为传统开口谐振环提出了一种简单实用的 Q 因子优化方法。

关键词: 太赫兹传感器; 超材料; 远红外; 品质因子 Q

中图分类号: O434.3

文献标识码: A

Introduction

Far-infrared rays (FIR) are electromagnetic waves within the wavelength range of 4-1 000 μm ^[1]. Given that most vibration and rotation frequencies of biomolecules fall within the FIR region, the resonance absorption of far-infrared waves provides a fingerprint spectrum corresponding to biomolecules. Analyzing the wavenumber and intensity of these characteristic resonance peaks, the qualitative identification and quantitative analysis of biological molecules can be realized^[2]. In addition, the photon energy of FIR rays is only 10^{-3} eV^[3], significantly lower than the energy required for molecular ionization^[4], eliminating ionization hazards to the human body and bio-

logical tissues^[5-6]. Therefore, far-infrared technology has found widespread applications in biomedical detection^[7-10], such as cancer cell detection^[11-12], drug recognition^[13], and virus rapid detection^[14].

Despite the versatile applications of traditional far-infrared technology in biomedical detection, it encounters challenges, particularly in detecting trace biomolecules due to insufficient sensitivity. Traditional FIR spectroscopy exhibits sensitivity in the milligram range, while the concentration of biomarkers in biological samples is usually in the microgram range or even the nanogram range. Thus, the far-infrared characteristic absorption peaks of biomarkers are often too weak to be identi-

Received date: 2023- 09- 19, revised date: 2023- 12- 19

收稿日期: 2023- 09- 19, 修回日期: 2023- 12- 19

Foundation items: Supported by the National Key Research and Development Program of China (2022YFA1404004, 2023YFF0719200); the National Natural Science Foundation of China (61805140, 62335012, 61988102).

Biography: LU Xiao-Sen (2002-), male, Shanghai, Bachelor. Research area involves Terahertz biosensors and application. E-mail: stg_shinra@163. com.

* **Corresponding author:** E-mail: wuxu@usst. edu. cn

fied and quantified accurately^[15]. To address this limitation, recent advancements in far-infrared biosensors have used metamaterials to enhance the resonance effect between molecules and FIR waves^[16-17]. These metamaterial-based biosensors have shown promise in improving the sensitivity of biomolecular detection^[18-20]. Importantly, metamaterials are easy to prepare, handle, and select^[21], making them ideal materials for developing highly sensitive biomedical sensors^[22-25].

In metamaterial biosensors, the quality factor Q (Q factor) is the critical performance indicator for evaluating sensor sensitivity^[26-28]. The Q factor closely correlates with the resonance properties of the resonator, including surface electrical field and resonant peak. A higher Q factor represents lower signal loss, improved signal localization, stronger resonance between the signal and the target analytes, and consequently, higher identification accuracy of target analytes^[29]. Various theoretical mechanisms underpin metamaterials, including inductive-capacitive (LC) resonance^[30], Fano resonance^[31], electromagnetically induced transparency (EIT)^[32-33], and bound-states in the continuum (BIC)^[34-35]. However, BIC metamaterial often face challenges in achieving the theoretical high Q resonance during production (need nanofabrication)^[36]. Metamaterials based on the Fano resonance and EIT mechanisms typically require complex resonance units and 2D nanomaterials (e. g., graphene) to improve the Q factor, but these approaches are impractical for mass production. Metal split-ring resonators based on the LC mechanism currently stand as the maturest metamaterial sensors and have been found widely applied in bio-detection. According to literatures^[37-41], adjustments to gap width and resonant shape (round, square, etc.) can modify resonance frequency and other sensing characteristics. Nevertheless, the impact of gap shape on the sensing characteristics of the split-ring resonator remains unexplored. In this paper, we take the double split-ring resonator based on the LC effect as an example, and analyze and discuss the influence of tip shape (angle and length) on the resonance properties. The results show that adjusting the gap shape to a sharp tip effectively improves the resonance properties, including electrical field strength, Q factor, and detection sensitivity. Finally, we propose an asymmetric tip design to optimize far-infrared metamaterial biosensors.

1 Design and Theory

1.1 Theoretical simulation

Theoretical simulations were performed using the COMSOL 5.4 software. The periodical boundary conditions with Floquet were applied in the x - and y -directions of a basic unit, and the open boundary condition was used in the z -direction along with the propagation direction of the incident wave.

1.2 Structural design

A typical metal double split-ring resonator structure based on the LC mechanism was selected for the asymmetric tip design. The metamaterial is composed of a metal double-split ring unit cell array and a substrate lay-

er. Its three-dimensional structure is shown in Fig. 1. Each resonant ring cell is attached to the substrate, and the period length of the cell structure is $a = 15 \mu\text{m}$. The substrate material is chosen to be polytetrafluoroethylene (PTFE), with a relative permittivity of 3.9, and the thickness of the substrate is $d = 2 \text{ mm}$. The material of the metal resonator is gold, which is set to be an ideal electrical conductor in the simulation model. The structural parameters of the resonator are given as follows: thickness $t = 50 \text{ nm}$, length $b = 10 \mu\text{m}$, width $w = 1 \mu\text{m}$, and gap $g_1 = g_2 = 1 \mu\text{m}$. The asymmetric tip design is carried out as follows: gap g_2 maintains its square structure, while gap g_1 changes its shape from square to tip by adjusting its angle (θ), from 16° to 180° .

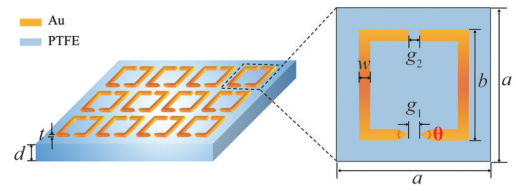


Fig. 1 Structural parameters of asymmetrically tipped split-ring resonator

图 1 开口谐振环的非对称针尖设计结构参数

1.3 Theoretical analysis

Typical split-ring resonators are inherently asymmetric. This asymmetry results in a potential difference between their left and right parts along the axis of the electric field, leading to an oscillating current according to the LC effect. Each ring resonator forms an LC oscillating circuit. The split gap represents a capacitance, and the metal ring can be equivalent to an inductance, as depicted in Fig. 2(a). The resonance frequency (ω_{LC}) can be calculated according to Equation (1):

$$\omega_{LC} = (LC)^{-\frac{1}{2}} = \frac{1}{\sqrt{L} \sqrt{\varepsilon_0 \int_0^v \varepsilon(\nu) E(\nu) d\nu}}, \quad (1)$$

Where L is the inductance, C is the capacitance, ε_0 is dielectric constant of vacuum, $E(\nu)$ is the electric field strength at the gap, and $\varepsilon(\nu)$ is the dielectric constant at different electric field strengths. The inductance (L) and capacitance (C) are affected by the geometrical parameters of the ring resonator^[42]. Altering the gap shape modifies the effective cross-section of the metal ring axis, causing changes in the capacitance (C).

Herein, a double-split square ring is used to study the influence of gap shape on the resonance properties. Fig. 2(b) shows the relationship between the tip length and tip angle of the gap g_1 . Due to structural limitations, 16° is the minimum achievable tip angle. As the tip angle gradually decreases, the tip length increases, with an accelerating rate. Based on the LC effect (Fig. 2(a)), the gaps g_1 and g_2 are equivalent to capacitance C_1 and C_2 , respectively, while the metal rings are equivalent to inductance L_1 and L_2 , respectively. Notably, the asymmetric tip design has a negligible impact on the equiva-

lent inductance L_1 and L_2 , but it does influence the equivalent capacitance C_1 . This will lead to changes in the resonant peak (Equation (1)). Changes in the resonant peak include the resonance wavenumber k_{WN} and the full width at half maximum X_{FWHM} , closely associated with the Q factor of split-ring resonators. The Q factor, determining the sensing sensitivity of metamaterials, is defined by Equation (2):

$$Q = \frac{0.03k_{\text{WN}}}{X_{\text{FWHM}}}, \quad (2)$$

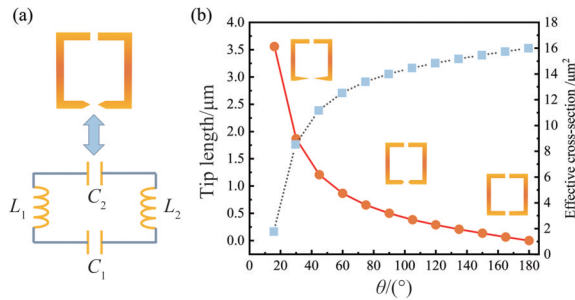


Fig. 2 Schematic of asymmetric tip design for far-IR metamaterial: (a) Schematic of equivalent capacitance and inductance effect; (b) Relationship between the tip length, tip area and the tip angle.

图2 远红外超材料的非对称针尖设计示意图:(a) 等效电容电感示意图;(b) 针尖长度、针尖面积和针尖角度之间的关系

2 Results and Discussions

2.1 Effect of asymmetric tip angle on the surface electric field

Firstly, we investigated the impact of an asymmetric tip on the surface electric field distribution of double split-ring resonators through theoretical simulation. The tip angles of the gap g_1 are classified into three categories: obtuse angles (180° , 150° , 120°), approximate right angles (105° , 90° , 75°), and acute angles (60° , 30° , 16°). Fig. 3 demonstrates that the electric field of the resonator consistently concentrates at the gap, especially at the edge of the metal ring, regardless of whether the shape of the gap is regular (180°) or sharp (not 180°). For resonators with the asymmetric tip, as shown in Fig. 3(b-i), the electric field strength at the gap g_1 (sharp tip, not 180°) is always higher than those at the g_2 gap (regular sharp, 180°). Furthermore, we found that when the tip angle approaches a right angle, the electric field strength of the resonator is slightly higher than that of resonators with acute or obtuse angles. According to the literature^[43], changes in the electric field distribution are closely linked to the geometric parameters of resonators. As the tip angle decreases from 180° to 90° , there is a slight increase in tip length (Fig. 2(b)), resulting in a more concentrated local electric field. However, further reducing the tip angle to 16° leads to a rapid change in tip length (Fig. 2(b)), causing field diffusion at the edges of the tip and a decrease in electric field strength.

These results indicate that the asymmetric tip design

does not change the theoretical mechanisms of the splitting resonator, but it amplifies the electric field strength. This is because it alters the shape of the metal layer, which directly affects the behavior of free electrons in the metal. As a result, under resonance conditions, this shape change facilitates easier excitation of free electrons by incident light and enhances the local electric field.

2.2 Effect of asymmetric tip angle on the resonance peak

Then, we studied the impact of an asymmetric tip on the resonance absorption peaks of double split-ring metamaterials. The far-infrared resonance spectra, obtained through theoretical simulations, as shown in Fig. 4. Curve (12) depicts the resonance peak of the untipped metamaterial ($\theta=180^\circ$), with a far-infrared resonance wavenumber of 259.74 cm^{-1} . Curves (1) - (11) represent the resonance peaks of the metamaterial with different tip angles at the gap g_1 , ranging from 261 to 273 cm^{-1} . Compared to the untipped structure, the resonance wavenumber of the asymmetric tip structure exhibits a blue shift. Additionally, the resonance wavenumber increases as the tip angle decreases. Notably, the rate of increase in resonance wavenumber is uneven despite a uniform decrease in the tip angle, aligning with the change in tip length depicted in Fig. 2(b). This illustrates that the resonance wavenumber change is primarily affected by the tip length of the split-ring metamaterial. Compared with the untipped structure, the asymmetric tip structure exhibits a blue shift in resonance wavenumber. Notably, this increase is observed unevenly, despite a uniform decrease in the tip angle. This trend aligns closely with the variation in tip length and tip area depicted in Fig. 2(b). This can be attributed to the gradual reduction of the tip angle, resulting in a decrease in the effective cross-sectional area at both ends of gap g_1 . As a consequence, the equivalent capacitance at gap g_1 diminishes gradually. According to Equation (1), this reduction in equivalent capacitance causes an increase in the resonant frequency. This phenomenon emphasizes that the change in resonance wavenumber is primarily influenced by the asymmetric tip design of the split-ring metamaterial.

Fig. 5(a) illustrates the changes in the FWHM of the resonance peak for materials at different tip angles. Fig. 5(b) shows the relationship between the FWHM and the tip angle (θ). The FWHM decreases gradually from 16° to 90° , enlarges from 90° to 150° , and experiences a slight decrease as the tip angle approaches untipped (165° - 180°). The FWHM reaches its minimum at a 90° tip angle (1.522 cm^{-1}). In addition, the FWHM is nearly flat when the tip angles are complementary to each other (e. g., 30° vs. 150° , 45° vs. 135° , 60° vs. 120° , and 75° vs. 105°). These changes in FWHM can be represented by a sine function: $\text{FWHM}=4.7+3.3\sin(\pi(\theta+6.1)/61.4)$, with a fitting coefficient of 0.89. This observed phenomenon likely correlates with the distribution of the electric field on the metasurface. As the tip angle gradually decreases from 180° to 90° , the local

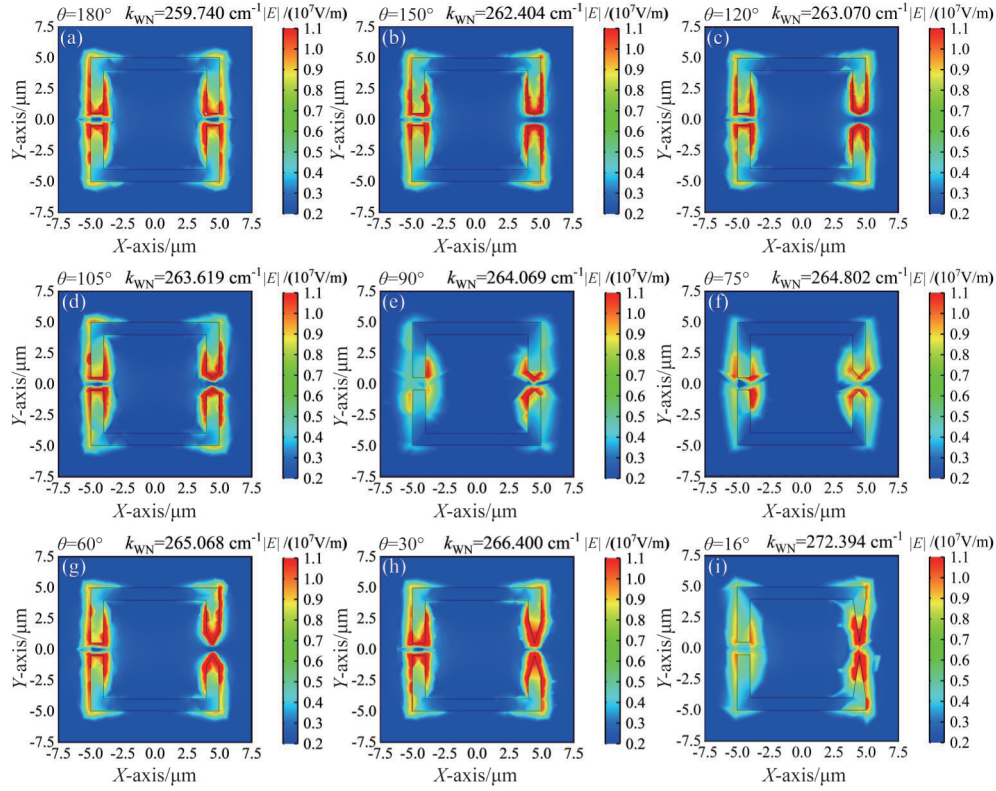


Fig. 3 Surface electric field distribution of far-IR metamaterial: (a) untipped structure; (b-i) asymmetric tip structure. The tip angle is (b) 150°; (c) 120°; (d) 105°; (e) 90°; (f) 75°; (g) 60°; (h) 30°, and (i) 16°, respectively

图3 远红外超材料的表面电场分布图: (a) 传统结构; (b-i) 非对称针尖结构. 针尖角度分别为 (b) 150°; (c) 120°; (d) 105°; (e) 90°; (f) 75°; (g) 60°; (h) 30°和 (i) 16°

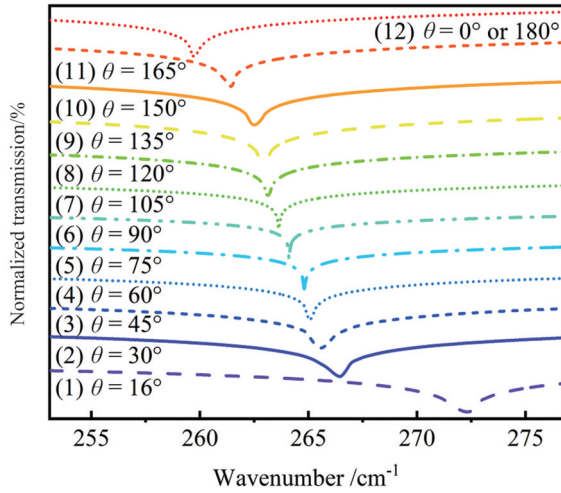


Fig. 4 Resonance wavenumber under different asymmetric tip angles (normalized resonant peaks separated in the vertical axis)

图4 不同非对称针尖角度下超材料的谐振波长(谐振峰经归一化处理并沿纵轴等间距分离)

electric field concentrates (Fig. 2 (a-e)). The heightened concentration enables the metamaterial to more efficiently respond to specific frequencies of electromagnetic waves, resulting in sharper resonance peaks. Further reduction in the tip angle to 16° induces diffusion of the local electric field at the edges of the tip due to increased tip length (Fig. 2 (f-i)), resulting in wider resonance

peaks and an increase in FWHM. Based on these results, it is clear that adjusting the tip angle of the gap g_1 between 60° and 120° effectively reduces the FWHM of resonance peaks. This reduction in FWHM will help improve the identification accuracy of the peak shifts in future sensing applications.

2.3 Effect of asymmetric tip angle on Q factor and sensing sensitivity

The relationship between the Q factor and the tip angle (θ) is depicted in Fig. 6. When the tip angle is untipped (180° or 0°), the Q factor of the double split-ring resonator is 51.59. However, as the tip angle increases from 16° to 165°, the Q factor goes through an increase, followed by a decrease, and then a slight increase. Notably, when the tip angle is 90°, the Q factor reaches its maximum at 173.52, which is three times greater than the Q factor of the untipped structure. This result suggests that the asymmetric tip design significantly enhances the Q factor of a double split-ring resonator, with optimal performance achieved at a 90° angle. The changes in the Q factor can be represented by a sine function: $y = 76.0 + 55.2 \sin(\pi(\theta - 57.5)/63.1)$, with a fitting coefficient of 0.83. According to Equation (2), the Q factor exhibits a direct proportionality to the resonance frequency and an inverse proportionality to the FWHM. As the tip angle decreases, there is a reduction in the effective cross-sectional area of the metal tip, leading to an increase in the effective capacitance C_1 . This, in turn, re-

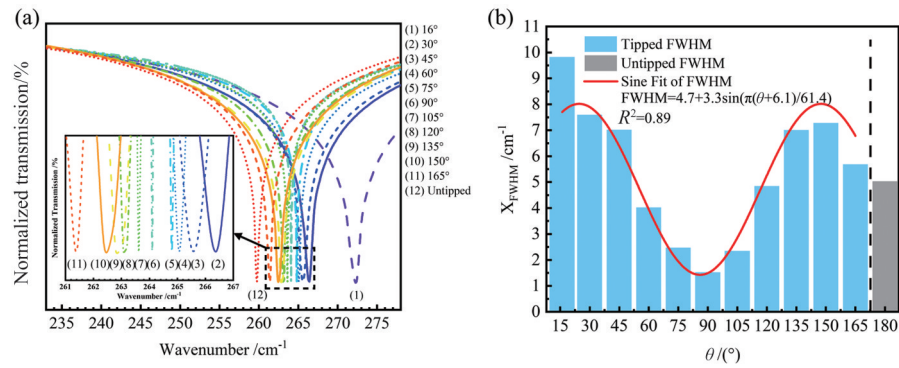


Fig. 5 FWHM under different asymmetric tip angles: (a) Normalized spectra; (b) Relationship between FWHM and tip angle
图5 不同非对称针尖角度下超材料谐振峰的半峰全宽: (a) 归一化谐振吸收谱; (b) 半峰全宽与针尖角度之间的关系

sults in a monotonous increase in the resonance frequency. Simultaneously, alterations in the electric field distribution cause the FWHM to initially decrease, followed by an increase. Ultimately, the relationship between the Q factor and the tip angle demonstrates non-monotonic behavior, characterized by an initial increase followed by a subsequent decrease.

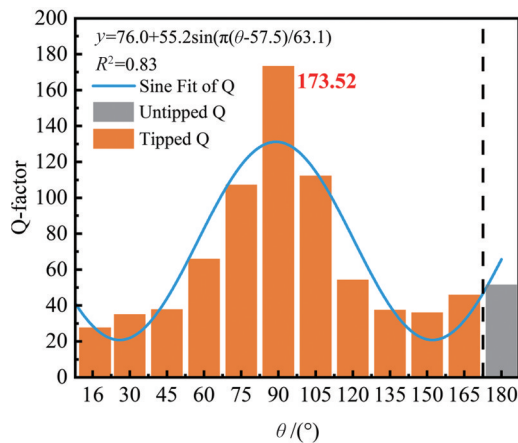


Fig. 6 Q factors of the double split-ring resonators under different asymmetric tip angles.
图6 不同非对称针尖角度下双开口谐振环的品质因子Q

To investigate the impact of asymmetric tip structures on the sensing sensitivity of metamaterials, we constructed a series of simulation experiments on untipped and tipped metamaterials (with a 90° angle). A sample layer was constructed on the surface of the metamaterial (Fig. 7(a)). The sample thickness (T) represents the amount of the target analyte. The dielectric constant (n) of the sample layer is fixed at 2.0 and 3.6, respectively, since the refractive indices of the majority of biomolecules fall within this range. Fig. 7(b-c) illustrate the relationships between the resonance peak of metamaterials and the thickness of the sample layer. The results indicate that, as the sample thickness increases, the resonant frequencies of the metamaterials exhibit a consistent redshift, and the frequency shift ultimately reaches a saturation value. It is noteworthy that when the sample thickness is small, the frequency shift of the tipped meta-

material is larger than that of the untipped metamaterial. Conversely, when the sample thickness is large, the frequency shift saturation of the tipped metamaterial is noticeably greater than that of the untipped metamaterial. These phenomena are more pronounced in low-index samples ($n=2.0$) compared to high-index samples ($n=3.6$). These observations suggest that the asymmetric tip structure exhibits higher sensitivity in detecting low-concentration biological samples, and this improvement closely depends on the dielectric constant of the sample.

3 Conclusions

This study focuses on the impact of asymmetric tip design on the resonance properties of typical double-split metal square ring, in the far-infrared region. The electric field distribution, resonance frequency, FWHM of the resonance peak, Q factor, and sensing sensitivity are all analyzed. The results indicate that asymmetric tip design enhances the electric field strength at the gap. As tip angle increases, the resonance frequency exhibits a redshift, the FWHM firstly decreases and then increases, while the Q factor firstly increases and then decreases. Notably, at a 90° angle, the Q factor reaches a maximum of 173.52—over three times higher than the untipped resonator with identical structural parameters. This work proposes an asymmetric tip design that significantly enhances the Q factor and sensing sensitivity. This strategy can be extended to various metal split-ring resonator structures.

References

- [1] Liou J C, Hsiao Y C, Yang C F. Infrared sensor detection and actuator treatment applied during hemodialysis [J]. *Sensors*, 2020, **20** (9): 2521.
- [2] Cheon H, Yang H J, Son J H. Toward clinical cancer imaging using terahertz spectroscopy [J]. *IEEE Journal of Selected Topics in Quantum Electronics*, 2017, **23**(4): 1–9.
- [3] Jin Z, Peng Y, Fang Y, et al. Photoinduced large polaron transport and dynamics in organic – inorganic hybrid lead halide perovskite with terahertz probes [J]. *Light: Science & Applications*, 2022, **11** (1): 209.
- [4] Yang J, Qi L M, Wu L Q, et al. Research progress of terahertz metamaterial biosensors [J]. *Spectroscopy and Spectral Analysis*, 2021, **41** (6): 1669–1677.
- [5] Wong C H, Lin L C, Lee H H, et al. The analgesic effect of thermal therapy after total knee arthroplasty [J]. *The Journal of Alternative and Complementary Medicine*, 2012, **18**(2): 175–179.

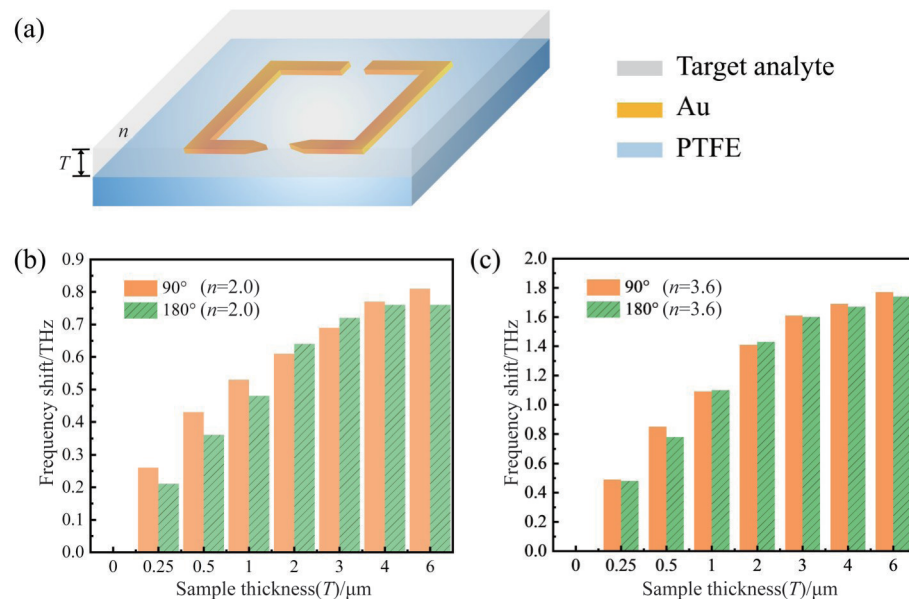


Fig. 7 Sensing sensitivity of the double split-ring resonators under different asymmetric tip angles: (a) Schematic of simulation model. The dielectric constant is (b) 2.0 and (c) 3.6, respectively

图 7 双开口谐振环在不同非对称针尖角度下的传感灵敏度: (a) 仿真模型; 模型中待分析物介电常数分别为 (b) 2.0 和 (c) 3.6

- [6] Leung T K. In vitro and in vivo studies of the biological effects of bio-ceramic (a material of emitting high performance far-infrared ray) irradiation [J]. *Chinese Journal of Physiology*, 2015, **58** (3): 147–155.
- [7] Zhang S, Chen X, Liu K, *et al.* Nonvolatile reconfigurable terahertz wave modulator[J]. *Photonix*, 2022, **3**(1): 1–14.
- [8] Barth A, Zscherp C. What vibrations tell about proteins[J]. *Quarterly Reviews of Biophysics*, 2002, **35**(4): 369–430.
- [9] Chan W L, Deibel J, Mittleman D M. Imaging with terahertz radiation[J]. *Reports on Progress in Physics*, 2007, **70**(8): 1325.
- [10] Zhao Y, Yang Y, Sun H B. Nonlinear meta-optics towards applications[J]. *Photonix*, 2021, **2**: 1–20.
- [11] Shi C J, Wu X, Peng Y. Applications of terahertz imaging technology in tumor detection[J]. *Opto-Electronic Engineering*, 2020, **47**(5): 190638.
- [12] Peng Y, Huang J, Luo J, *et al.* Three-step one-way model in terahertz biomedical detection[J]. *Photonix*, 2021, **2**(1): 1–18.
- [13] Cai X, Sushkov A B, Suess R J, *et al.* Sensitive room-temperature terahertz detection via the photothermoelectric effect in graphene[J]. *Nature Nanotechnology*, 2014, **9**(10): 814–819.
- [14] Falconer R J, Markelz A G. Terahertz spectroscopic analysis of peptides and proteins[J]. *Journal of Infrared, Millimeter, and Terahertz Waves*, 2012, **33**: 973–988.
- [15] Gu H, Shi C, Wu X, *et al.* Molecular methylation detection based on terahertz metamaterial technology [J]. *Analyst*, 2020, **145** (20): 6705–6712.
- [16] Nan J J. Novel surface plasmon resonance nanostructure and its application in biological sensing [D]. Changchun: Jilin University, 2020: 13–22.
- [17] Wang Z L. A review on research progress in surface plasmons [J]. *Progress in Physics*, 2009, **29**(3): 287–324.
- [18] Pal S, Prajapati Y K, Saini J P, *et al.* Sensitivity enhancement of metamaterial-based surface plasmon resonance biosensor for near infrared[J]. *Optica Applicata*, 2016, **46**(1): 131–143.
- [19] Eleftheriades G V, Siddiqui O, Iyer A K. Transmission line models for negative refractive index media and associated implementations without excess resonators[J]. *IEEE Microwave and Wireless Components Letters*, 2003, **13**(2): 51–53.
- [20] Yao J, Ou J Y, Savinov V, *et al.* Plasmonic anapole metamaterial for refractive index sensing[J]. *Photonix*, 2022, **3**(1): 23.
- [21] Liu K, Zhang R, Liu Y, *et al.* Gold nanoparticle enhanced detection of EGFR with a terahertz metamaterial biosensor[J]. *Biomedical Optics Express*, 2021, **12**(3): 1559–1567.
- [22] Jin Z, Peng Y, Ni Y, *et al.* Cascaded amplification and manipulation of terahertz emission by flexible spintronic heterostructures[J]. *Laser & Photonics Reviews*, 2022, **16**(9): 2100688.
- [23] Yu N, Capasso F. Flat optics with designer metasurfaces[J]. *Nature Materials*, 2014, **13**(2): 139–150.
- [24] Deng X X, Shen Y C, Liu B W, *et al.* Terahertz metamaterial sensor for sensitive detection of citrate salt solutions[J]. *Biosensors*, 2022, **12**(6): 408.
- [25] Ma J L, Tang J C, Wang K C, *et al.* A THz-TDS based metamaterial sensor for the sensitive distinguishment of food additives[J]. *Journal of Infrared and Millimeter Waves*, 2022, **41**(3): 581–588.
- [26] Ding C F. Research on THz metamaterials with high-Q resonance [D]. Tianjin: Tianjin University, 2016: 9–13.
- [27] Xiao M, Lang T, Ren Z, *et al.* Flexible graphene-based metamaterial sensor for highly sensitive detection of bovine serum albumin[J]. *Applied Optics*, 2022, **61**(35): 10574–10581.
- [28] Ma L, Chen D, Zheng W, *et al.* Thermally tunable high-Q metamaterial and sensing application based on liquid metals[J]. *Optics Express*, 2021, **29**(4): 6069–6079.
- [29] Wang H C, Chen J, Dong G M, *et al.* Early rub-impact diagnosis of rotors based on tunable Q-factor wavelet transformation[J]. *Journal of Vibration and Shock*, 2014, **33**(10): 77–80.
- [30] Zhou J, Koschny T, Kafesaki M, *et al.* Saturation of the magnetic response of split-ring resonators at optical frequencies[J]. *Physical Review Letters*, 2005, **95**(22): 223902.
- [31] Ding S Y, Yi J, Li J F, *et al.* Nanostructure-based plasmon-enhanced Raman spectroscopy for surface analysis of materials[J]. *Nature Reviews Materials*, 2016, **1**(6): 1–16.
- [32] Yang Y, Kravchenko I I, Briggs D P, *et al.* All-dielectric metasurface analogue of electromagnetically induced transparency[J]. *Nature Communications*, 2014, **5**(1): 5753.
- [33] Lyu J M, Shen S Y, Chen L, *et al.* Frequency selective fingerprint sensor: the Terahertz unity platform for broadband chiral enantiomers multiplexed signals and narrowband molecular AIT enhancement[J]. *Photonix*, 2023, **4**(1): 28.
- [34] Carletti L, Koshelev K, De Angelis C, *et al.* Giant nonlinear response at the nanoscale driven by bound states in the continuum[J]. *Physical Review Letters*, 2018, **121**(3): 033903.
- [35] Wang R, Xu L, Huang L, *et al.* Ultrasensitive terahertz biodetection enabled by quasi-BIC-based metasensors[J]. *Small*, 2023: 2301165.
- [36] Wang Y, Han Z, Du Y, *et al.* Ultrasensitive terahertz sensing with high-Q toroidal dipole resonance governed by bound states in the continuum in all-dielectric metasurface[J]. *Nanophotonics*, 2021, **10**(4): 1295–1307.
- [37] Okamoto T, Otsuka T, Sato S, *et al.* Dependence of LC resonance wavelength on size of silver split-ring resonator fabricated by nanosphere lithography[J]. *Optics Express*, 2012, **20** (21): 24059–24067.
- [38] Driscoll T, Andreev G O, Basov D N, *et al.* Tuned permeability in

- terahertz split-ring resonators for devices and sensors [J]. *Applied Physics Letters*, 2007, **91**(6): 2511.
- [39] Baena J D, Bonache J, Martin F, *et al.* Equivalent-circuit models for split-ring resonators and complementary split-ring resonators coupled to planar transmission lines [J]. *IEEE Transactions on Microwave Theory and Techniques*, 2005, **53**(4): 1451–1461.
- [40] Corrigan T D, Kolb P W, Sushkov A B, *et al.* Optical plasmonic resonances in split-ring resonator structures: An improved LC model [J]. *Optics Express*, 2008, **16**(24): 19850–19864.
- [41] Asgari S, Fabritius T. Graphene-based multiband chiral metamaterial absorbers comprised of square split-ring resonator arrays with different numbers of gaps, and their equivalent circuit model [J]. *IEEE Access*, 2022, **10**: 63658–63671.
- [42] Xiong Z, Shang L, Yang J, *et al.* Terahertz sensor with resonance enhancement based on square split-ring resonators [J]. *IEEE Access*, 2021, **9**: 59211–59221.
- [43] Liu B, Peng Y, Jin Z, *et al.* Terahertz ultrasensitive biosensor based on wide-area and intense light-matter interaction supported by QBIC [J]. *Chemical Engineering Journal*, 2023, **462**: 142347.